Journal of Physics: Conference Series

PAPER • OPEN ACCESS

Experimental investigation on flow boiling heat transfer and pressure drop of refrigerants R32 and R290 in a stainless steel horizontal tube

To cite this article: B Citarella *et al* 2019 *J. Phys.: Conf. Ser.* **1224** 012041

IOP Conf. Series: Journal of Physics: Conf. Series **1224** (2019) 012041 doi:10.1088/1742-6596/1224/1/012041

Experimental investigation on flow boiling heat transfer and pressure drop of refrigerants R32 and R290 in a stainless steel horizontal tube

B CITARELLA, G LILLO, R MASTRULLO, A W MAURO and L VISCITO

Department of Industrial Engineering, Federico II University of Naples, P.le Tecchio 80, 80125, Naples (Italy)

E-mail: alfonsowilliam.mauro@unina.it

Abstract. The purpose of this paper is to present new flow boiling heat transfer and pressure drop data in a single, horizontal smooth stainless steel tube of 6.0 mm internal diameter, in which R32 and R290 (propane) are employed as working fluids. The cross sectional average heat transfer coefficients are obtained by measuring the temperatures at the top, bottom, left and right sides of the channel. The experimental trends are analyzed for different operating conditions in terms of mass velocity (from 150 to 300 kg/(m^2 s)) and heat flux (from 10 to 40 kW/m^2). The saturation temperature is fixed to 25 °C for the heat transfer data and to 25 and 35 °C for the pressure drop experiments. The effects of the operative parameters and of the working fluids on local heat transfer coefficients and frictional pressure drop are discussed and the experimental data are finally compared with some of the available correlations taken from scientific literature.

1. Introduction

The correct design of evaporators in domestic and commercial air conditioning and refrigeration systems continuously requests flow boiling heat transfer and pressure drop data, especially in case of low-GWP refrigerants that are about to replace the conventional HFC substances [1]. Propane (R290) might be an interesting alternative thanks to its excellent thermodynamic and transport properties and miscibility with usual compressor lubricants. Nevertheless, its use is often restricted to small plants with low fluid inventory due to its high flammability. On the other hand, R32 is currently used in residential and industrial air-conditioning systems as a substitute for R410A and it is also expected to be a component of R32/HFO mixtures in the next future [2].

Although the flammability of R290 and R32 may represent a safety issue, the latent heat of these fluids is almost double of that of typical synthetic refrigerants, thus allowing the use of a considerably reduced mass flow rate required compared to HFCs fluids for the same amount of heat duty without affecting the system performance. On this regard, Mastrullo et al. [3] proposed R290 as working fluid in a light vertical freezer for commercial applications. The authors found that the refrigerant charge could be kept below the limits allowed by the current standards and also that the overall performance was increased with respect to the baseline configuration with refrigerant R410A. Later on, Fernando et al. [4] found that a 5 kW water-to-water heat pump could be run with only 200 g of propane without

any penalization on the system performance when compared to a conventional design. Botticella et al. [2], in their multi-criteria optimization of a residential split system heat pump, found that refrigerant R32 is the most promising solution in terms of manufacturing costs, consumers' costs and environmental impact. Another research performed by Xu et al. [5] has pointed out that the coefficient of performance (COP) using R32 in a vapor-injected heat pump was increased up to 10% if compared to the R410A case operating under the same conditions.

Despite the wide range of possible applications for R290 and R32 as working fluids has been demonstrated, limited amount of heat transfer and pressure drop data are currently available in scientific literature. Recently, Longo et al. [6] provided flow boiling data of pure R290, propylene and R404A in a circular tube of 4.0 mm, exploring saturation temperatures from 5 to 20 °C, mass fluxes from 104 to 313 kg/(m^2 s) and heat fluxes from 15 to 31 kW/m^2. The authors found a nucleate boiling prevalent behaviour, with heat transfer coefficients not affected by a change of vapor quality especially at low mass fluxes and high heat fluxes and saturation temperatures.

Wang et al. [7] performed flow boiling experiments with R290 in a 6.0 mm horizontal tube, with low saturation temperatures (from -35 to -2 °C) and low mass fluxes (from 62 to 104 kg/(m^2 s)). The heat transfer performance was seen to be increased with mass flux at high vapor qualities and with saturation temperature at high heat fluxes, which positively affected the heat transfer coefficients in any condition.

For smaller pipes, Del Col et al. [8] studied flow boiling heat transfer and pressure drop of R290 in a 0.96 mm channel at a fixed saturation temperature of 31 °C. All the prediction methods chosen by the authors underestimated the heat transfer coefficient trends.

Flow boiling of R32 in a 4.0 mm internal diameter horizontal tube has been experimentally investigated by Longo et al. [9] for three saturation temperatures (5, 10 and 20 °C). The heat transfer coefficient was seen to be nearly independent on vapor quality and mass flux, whereas a higher sensitivity for heat flux variations was observed, especially at higher saturation temperatures.

Jige et al. [10] investigated the effect of the tube diameter on flow boiling heat transfer and pressure drop of R32 in small channels of 1.0, 2.2 and 3.5 mm internal diameters, at a fixed saturation temperature of 15 °C and by varying heat and mass flux. No differences were found on the heat transfer mechanisms with respect to conventional macro-tubes, and the heat transfer coefficients were seen to be higher with lower internal diameters under the same experimental conditions. Higher pressure drops were instead recorded for lower tube diameters and higher mass fluxes.

In this paper, new flow boiling heat transfer coefficient and pressure drop data of R290 and R32 are provided in a horizontal stainless steel tube of 6.0 mm internal diameter. Experiments were performed by investigating the effect of the operating parameters in terms of mass flux (from 150 to 300 kg/(m^2 s)) and heat flux (from 10 to 40 kW/m^2). The saturation temperature has been fixed to 25 °C for the heat transfer experiments and to 25 and 35 °C for the adiabatic frictional pressure gradient tests. Finally, the agreement with some prediction methods is also checked.

2. Experimental facility

The test facility for the flow boiling heat transfer and pressure drop experiments is schematically shown in Fig. 1, in which the refrigerant loop and the water cooling loop are displayed as black and blue lines, respectively.

The sub-cooled refrigerant passes through a magnetic gear pump, which is able to provide volumetric flow rates within a range of 1.3-2.5 dm^3/min by changing its rotating speed. The liquid mass flow rate is then measured by a Coriolis flow meter before the preheater section, which is made up of a copper tube where the heat is provided by means of four fiberglass heating tapes (each one with a nominal heat power of 900 W at 25 °C and 240 V). For the control of the local vapor quality at the test section inlet, the applied heat at the preheater section is managed thanks to a solid state relay and with the help of Arduino One controller. An adiabatic horizontal portion (40 cm) of stainless steel tube is provided in order to let the fluid be fully developed before the test section inlet. The saturated

vapor is then condensed in a plate heat exchanger and finally sub-cooled in a tube-in-tube heat exchanger before the pump suction head that closes the loop. Two different throttling valves are positioned on the liquid and vapor lines, respectively, and a bypass circuit is provided at the pump outlet in order to have multiple mass flow rate control options.

Demineralized water is the cooling fluid, whose temperature is controlled by a thermostatic bath. Both the tube-in-tube and the plate heat exchangers may be independently excluded from the water flow by means of two dedicated bypass circuits.

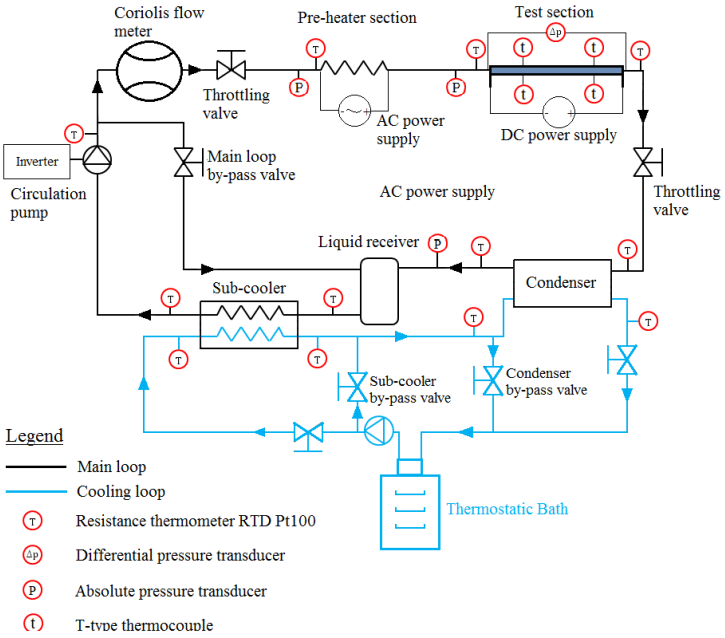

Figure 1. Schematic description of the experimental facility

2.1. Test section

All the flow boiling experiments have been conducted in a smooth, horizontal, circular stainless steel (AISI SS316) tube having an internal diameter of 6.00 ±0.05 mm and an external diameter of 8.00 ±0.05 mm. According to the tube manufacturer, the roughness of the inner surface is 10 μm. A photograph and the main characteristics of the tube test section are provided in Fig. 2. The heat flux is obtained by means of Joule effect provided by a DC power supply unit (within the range 0-8 V and 0-300 A) connected to the test section with two shorts copper wires clamped on copper electrodes welded on the tube surface (see points A and E in Fig. 2). The total measured heated length is 193.7±0.79 mm. At a distance of 237.5±0.91 mm, two pressure taps (points P and R) are provided for the measurement of the inlet absolute pressure and of the pressure drop across the test section. The local heat transfer coefficient is measured in the position C, at a distance of 146.7 ±0.64 mm from the inlet section. In this point, four T-type thermocouples are glued on the tube external surface with a high-conductivity epoxy resin, whereas a Kapton thin adhesive layer guarantees the electrical insulation from the heated channel [11]. The DC voltage for the evaluation of the imposed heat flux is measured between the position B and D in order to avoid locally concentrated tension drops in the electrodes proximity. Different layers of synthetic foam (λ = 0.040 W/(m K)) are used for the insulation of the test section and of the entire test facility, with the exception of the preheater section, which has been firstly covered with two layers of mineral wool (λ = 0.070 W/(m K)) due to the higher temperatures reached during the experimental procedure.

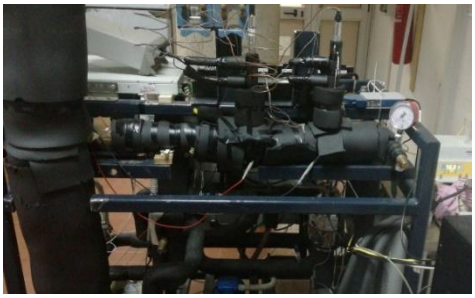

Geometrical features	
A, E	copper electrodes
B, D	voltage measurement points
C	temperature measurement point
AE	193.7 ±0.79 mm
BD	101.6 ±0.41 mm
AC	146.7 ±0.64 mm
d	6.00 ±0.05 mm (internal diameter)
D	8.00 ±0.05 mm (outer diameter)
PR	237.5 ±0.91 mm (pressure taps distance)
PC	166.9 ±0.91 mm

Figure 2. Photograph and geometrical details of the test section

2.2. Measurement instrumentation

Different RTDs are placed throughout the main and secondary loops for the measurement of the fluid temperature, carrying an overall uncertainty of ±0.180 °C. The wall temperature measurements for the evaluation of the heat transfer coefficients are instead obtained with four T-type thermocouples, calibrated *in-situ* with two resistance thermometers and a thermostatic bath. The overall estimated uncertainty for these sensors, by taking into account also the residual errors of the calibration curve, is assumed to be ±0.1 °C.

The absolute pressure at the test section inlet is measured with an absolute pressure transducer having a measuring range of 0-35 bar and an overall uncertainty of ±0.5% of the read value. The pressure drop is instead estimated with a differential pressure transducer, calibrated *in-situ* with a water liquid column and a yardstick. The instrumental uncertainty is estimated to be ±0.06 kPa.

The mass flow rate is measured by means of a Coriolis flow meter, calibrated up to 2% of the full scale, with a maximum uncertainty of ±1% of the measurement.

A digital wattmeter provides the heat applied to the preheater section, by separately measuring the voltage (100 mV-500 V) and current (1 mA-16 A). Its uncertainty is ±1.0% of the reading, as provided by the manufacturer.

The heat flux applied to the test section requires the measurement of the DC voltage (electrical voltage transducer within 0-5 V and an uncertainty of ±0.03% of the reading) and the DC current (directly measured by the DC power unit within 0-300 A and an uncertainty of ±1.0%).

2.3. Experimental procedure

The operating parameters in terms of mass flux, saturation temperature and heat flux are fixed at the beginning of each experiment, which starts from the onset of boiling and proceeds with increasing vapor quality up to the occurrence of dry-out, by means of the AC voltage applied to the fiberglass heating tapes of the preheater section. The test is stopped once the dry-out heat transfer is established (as soon as the heat transfer coefficient drops more than 25% from its previous value) and the wide wall temperature fluctuations would not guarantee high-quality experimental data.

The thermostatic bath control defines the saturation temperature of the system, whereas the inverter frequency of the electrical motor coupled with the magnetic gear pump changes the mass flow rate, which can be furtherly controlled by using the bypass circuit and/or the throttling valves on the liquid and vapor lines. Finally, the heat flux is imposed by setting the desired voltage of the DC power supply unit.

All the data are obtained in steady state conditions (with the exception of the dry-out points in which the phenomenon itself is time-dependent), with a recording frequency of 1.0 Hz. The nominal values of each sample are the arithmetic average of the measured quantities over a recording time of 90 s. The system is considered stabilized when the calculated deviation of the main parameters is sufficiently low (±2% for the mass velocity, ±0.1 °C for the saturation temperature).

3. Experimental method

3.1. Data reduction, uncertainty analysis and validation

The local heat transfer coefficient and the imposed heat flux are evaluated as follows:

$$h = \frac{q}{T_{wall} - T_{sat}} \tag{1}$$

$$q = \frac{V_{BD} \cdot I}{\pi d \overline{BD}} \tag{2}$$

where the subscripts *wall* and *sat* refer to the inner wall temperature and the local saturation temperature, respectively. The cross sectional average heat transfer coefficient shown in the results section is the arithmetical average of the four heat transfer coefficients obtained on the top, bottom, left and right sides of the test tube. V_{BD} is the voltage applied in the section *BD, I* is the DC current flowing in the test tube and *d* is the channel internal diameter. The fluid saturation temperature at the measurement point is obtained by considering a linear pressure drop profile from the tube inlet. The wall temperature is instead evaluated from the measured wall outer temperature T_{th} by considering 1-D heat transfer and uniform generation in the metal tube having λ_{tube} (16.26 W/(m K)) as thermal conductivity and *D* as external diameter:

$$T_{wall} = T_{th} + \frac{V_{BD} \cdot I}{4\pi\lambda_{tube} \overline{BD}} \cdot \frac{\left(\frac{D}{d}\right)^2 \cdot \left(1 - \ln\left(\left(\frac{D}{d}\right)^2\right)\right) - 1}{\left(\frac{D}{d}\right)^2 - 1} \tag{3}$$

The local vapour quality at the measurement point requires the knowledge of the local enthalpy, which is computable with an energy balance applied to the test section:

$$i = i_{in} + \frac{4 \cdot \overline{AC} \cdot q}{G \cdot d} \tag{4}$$

where *G* is the refrigerant mass flux and i_{in} is the test section inlet enthalpy, whose value is obtained from an energy balance applied to the preheater section, in which $i_{in,preh}$ is the preheater inlet enthalpy of the sub-cooled liquid, $\dot{Q}_{preh}$ is the preheater load and $\dot{m}$ is the refrigerant measured mass flow rate.

$$i_{in} = i_{in,preh} + \frac{\dot{Q}_{preh}}{\dot{m}} \tag{5}$$

All refrigerant thermodynamic properties are evaluated with the software REFPROP 9.0, whereas the whole data reduction is carried out with MATLAB software.

3.2. Uncertainty analysis and validation

The instrumental B-type uncertainties are composed to the standard deviation evaluated in the recording time for all the measured parameters. The uncertainty analysis of the derived results is then carried out by using the law of propagation of errors [11]-[12]. The maximum uncertainties are typically detected at the dry-out occurrence due to the higher fluctuations of the measured parameters. Lower uncertainty values are instead recorded during stable boiling. Tab. 1 shows the maximum and the average recorded uncertainty for the main operating parameters and results.

Table 1 Summary of the uncertainty analysis

Parameter	Average uncertainty	Maximum uncertainty
Saturation temperature T_{sat}	±0.05 °C	±0.08 °C
Mass flux G	±1.1%	±3.5%
Heat flux q	±0.70%	±0.76%
Vapor quality x	±0.04	±0.19
Mean heat transfer coefficient h_{mean}	±7.5%	±16%
Pressure gradient $\frac{\Delta P}{\Delta z}$	±1.8%	±11%

The preheater and test section insulation and the correct functioning of the whole experimental apparatus have been checked with liquid single-phase experiments by using refrigerant R134a. The electrical power (from 220 to 1460 W in the preheater section and from 10 to 150 W in the test section) is compared to the heat absorbed by the sub-cooled refrigerant by means of two energy balances performed in the heated sections. In all tests, the wall and ambient temperatures reached similar values than those obtained during the flow boiling experiments.

The liquid single-phase heat transfer coefficients for refrigerant R134a are also evaluated and compared to the well-known Dittus-Boelter prediction method [13]. Further detailed information on the validation procedure and results can be obtained from a previous work of the same authors with the same test facility [11].

4. Results

4.1. Heat transfer coefficient: experiments and assessment

The heat transfer coefficients points presented in this section are intended to be averaged over the four measurement points (top, bottom, left and right sides of the tube). The parameters and their uncertainties for all the titles and legends in the following diagrams are averaged over all the corresponding represented data.

In this experimental campaign, R32 and R290 are employed as working fluids and the saturation temperature has been fixed to 25 °C. Mass fluxes between 150 and 300 kg/(m^2 s) and heat fluxes from 10 to 40 kW/m^2 have been investigated and the effect of their variation on the local heat transfer coefficients is discussed in the following diagrams.

Fig. 3 shows the effect of the mass flux on the mean heat transfer coefficient. Fig. 3a refers to refrigerant R32 with an imposed heat flux of 10 kW/m^2 and Fig. 3b refers to propane (R290) with a heat flux of 20 kW/m^2. The heat transfer coefficients trends of R32 are different depending on the

mass flux: for the lower values of 152 and 223 kg/(m^2 s), the heat transfer performance is not particularly affected by vapor quality and also by a change of the mass flux itself, even if a slight deterioration of the heat transfer coefficient with ongoing evaporation is detected for the lowest mass flux investigated. A different trend is shown for the mass flux of 301 kg/(m^2 s), in which the heat transfer coefficient increases with vapor quality (passing from 6 to 10 kW/(m^2 K)) and exposes a typical convective behavior. The dry-out phenomenon occurs at higher vapor qualities with increasing mass velocity, passing from 0.79 to 0.86 when the mass flux is changed from 152 to 301 kg/(m^2 s).

The trends of R290 are similar to those displayed for refrigerant R32 and are not affected by the mass flux and vapor quality variations for all the operating conditions investigated, showing a nearly constant value of 9-10 kW/(m^2 K) from the onset of boiling up to the dry-out occurrence, which happens at approximately x = 0.85 for the three operating conditions shown.

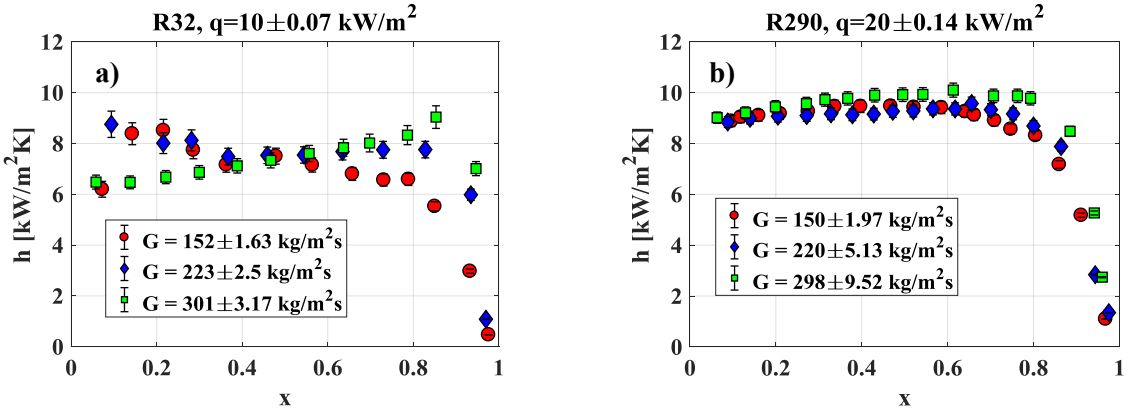

Figure 3. Effect of the mass flux on the mean heat transfer coefficient. The saturation temperature is fixed to 25 °C. (a) R32 with q = 10 kW/m^2; (b) R290 with q = 20 kW/m^2.

The effect of the imposed heat flux on the average heat transfer coefficients of R32 and R290 is shown in Fig. 4a-b, respectively. At a mass flux of 220 kg/(m^2 s) and with refrigerant R32, the heat transfer coefficient remains almost constant with ongoing evaporation when the vapor quality is included between 0.2 and 0.8 for the three curves shown. At lower vapor qualities, the heat transfer coefficient is nearly constant for a heat flux of 10 kW/m^2, whereas shows an increasing trend for q = 20 kW/m^2 and a decreasing trend for q = 40 kg/m^2. An increasing heat flux determines a significant increase of the average heat transfer coefficient (approximately +55% from 10 to 40 kW/m^2) at any vapor quality, suggesting a strong nucleate heat transfer contribution in these conditions. A higher imposed heat flux leads also to a progressive reduction of the vapor quality at the occurrence of dry-out, passing from 0.93 to 0.78.

A similar behavior is observed for refrigerant R290 at the same mass flux of 220 kg/(m^2 s), for which the dry-out occurrence is anticipated from 0.85 to 0.63 with increasing heat flux. For this fluid, the convective heat transfer is not completely suppressed due to the slight increase of the heat transfer coefficient with increasing vapor quality for all the heat fluxes investigated. The effect of the imposed heat flux is anyway more evident employing R290, with the average heat transfer coefficient that is almost doubled up when passing from 10 to 40 kW/m^2.

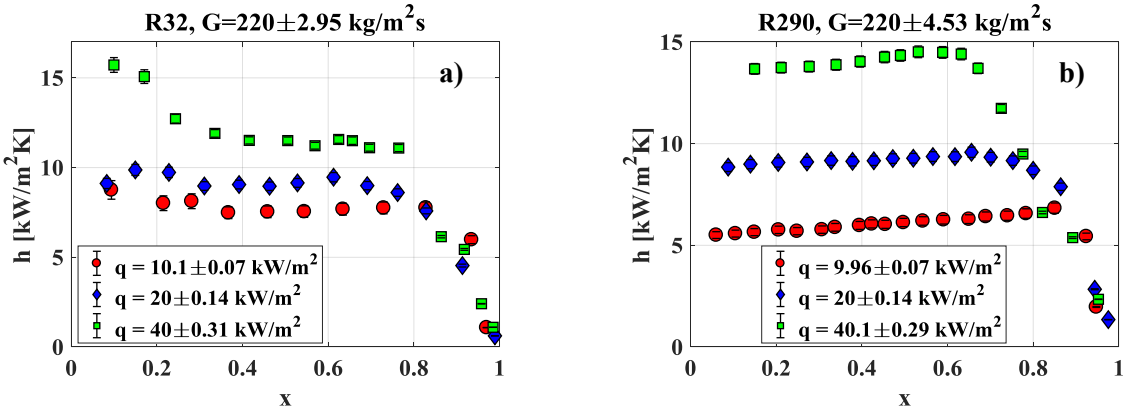

Figure 4. Effect of the heat flux on the mean heat transfer coefficient. The saturation temperature is fixed to 25 °C. (a) R32 with G = 220 kg/(m^2 s); (b) R290 with G = 220 kg/(m^2 s).

The experimental heat transfer coefficient data (including those after dry-out occurrence) are finally compared with two correlations taken from scientific literature. Particularly, the prediction methods of Wojtan et al. [14] and Del Col [15] are chosen for comparison. The statistic analysis and the graphical comparisons have been separately performed with the two refrigerants employed and are summarized in Fig. 5a-b.

The flow pattern based method of Wojtan et al. [14] was developed for macro-tubes by employing R410A as operating fluid. It works similarly for both refrigerants, providing a Mean Absolute Error (*MAE*) of 28.1% and 29.8% when applied to R32 and R290 data, respectively. The correlation of Del Col [15] is a modification of the original Gungor and Winterton [16] method, adapted for the author's data with halogenated refrigerants in a smooth horizontal tube of 8.0 mm internal diameter. From Fig. 5b, even if this method provides higher errors for higher heat transfer coefficients, it returns the best agreement with the experimental data, with a *MAE* equal to 19.6% for R32 and to 24.6% for the R290 heat transfer coefficient points.

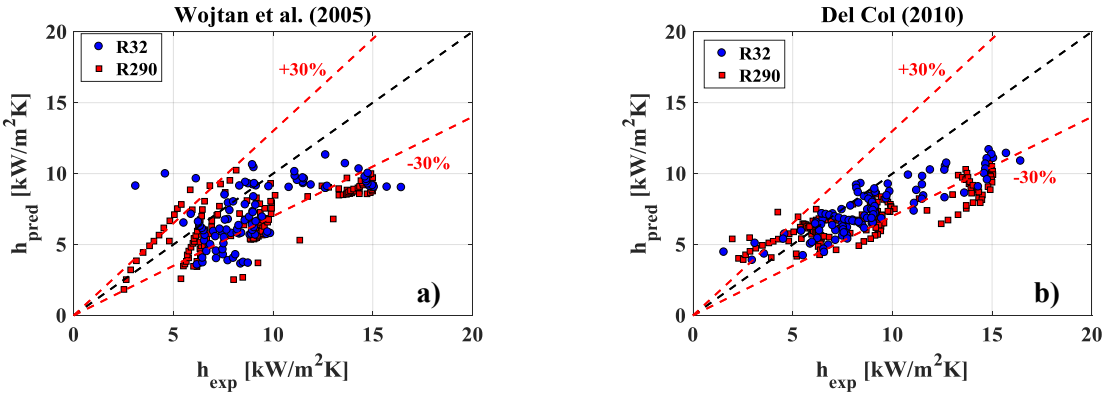

Figure 5. Experimental versus predicted heat transfer coefficients. Correlations of: (a) Wojtan et al. [14]; (b) Del Col [15]

4.2. Adiabatic pressure gradients: experiments and assessment

The effect of the saturation temperature and mass flux on the frictional pressure gradient is shown in Fig. 6a-b, respectively. The general trend is an increasing pressure drop with vapor quality, due to the flow acceleration, and then a decreasing trend after a peak value. For both fluids, an increase of the saturation temperature leads to a higher vapor phase density which in turn reduces the shear stress

between the two phases, resulting in a slight reduction of the pressure drop, especially in case of high vapor qualities, where the flow velocity is more substantial. For the same reason, the frictional pressure gradients of R32 (reduced pressure of 0.29 at 25 °C) are lower than those of R290 at the same operating conditions (reduced pressure of 0.22 at 25 °C).

The pressure drop is also significantly increased with mass flux due to a higher flow mean velocity and inertia: at x = 0.8, the pressure gradient of R32 at 35 °C for G = 301 kg/m^2 s is approximately 450% higher than that obtained for G = 151 kg/(m^2 s). Similar trends with mass velocity are also found for refrigerant R290.

The experimental frictional pressure drop data are finally compared with the values obtained from the separated flow models of Zhang and Webb [17] and Friedel [18]. The graphical comparison is shown in Fig. 7a-b, with different markers for the two fluids. The correlation of Zhang and Webb [17] better predicts the R32 data, with a calculated *MAE* of 21.5%, whereas for R290 the agreement is slightly worse (*MAE* = 27.8%). On the other hand, the model of Friedel [18] provides a lower *MAE* (equal to 21.4%) for the R290 data, whereas tends to overestimate most of the R32 points (*MAE* = 41.7% and *MRE* = +38.5%).

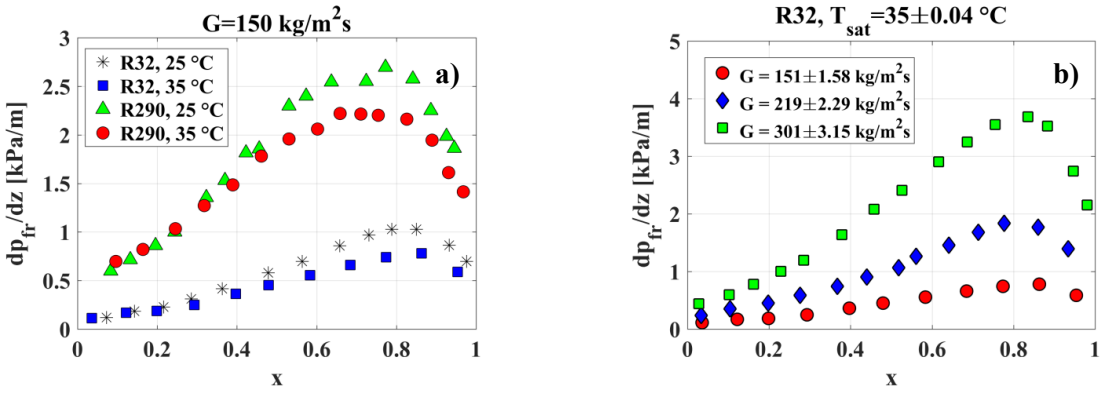

Figure 6. Experimental adiabatic frictional pressure gradients. (a) Saturation temperature effect for both fluids at G= 150 kg/(m^2 s); (b) Mass flux effect for R32 at T_{sat} = 35 °C

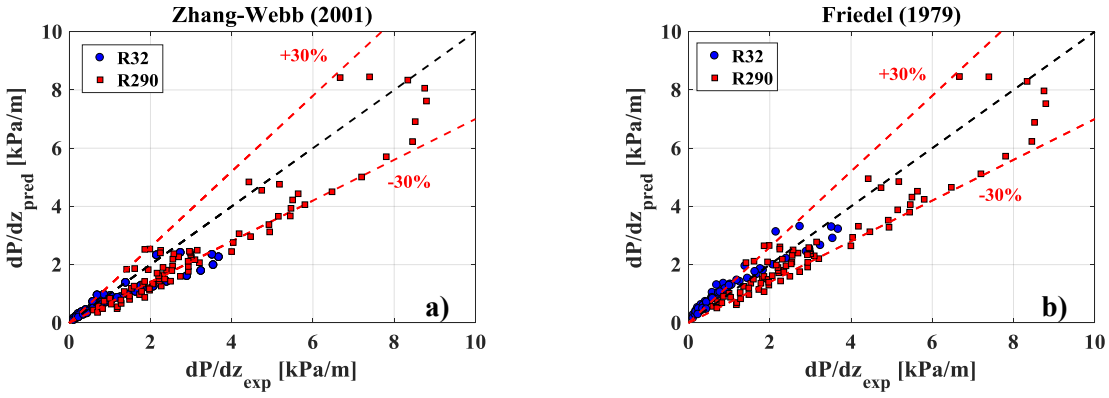

Figure 7. Experimental versus predicted frictional pressure gradients. Correlations of: (a) Zhang and Webb [17]; (b) Friedel [18]

5. Conclusions

New experimental data on local two-phase heat transfer coefficients and adiabatic pressure gradients for refrigerants R32 and R290 are obtained for a horizontal stainless steel tube of 6.0 mm internal

diameter. The effects of the heat and mass flux (from 10 to 40 kW/m^2 and from 150 to 300 kg/(m^2 s), respectively) on the heat transfer coefficient and of the mass flux and saturation temperature (fixed to 25 and 35 °C) on the frictional pressure gradients are investigated. The main conclusions may be summarized as follows:

- The heat transfer coefficients of R290 present an almost constant trend with vapor quality and are not affected by a change of the mass flux, suggesting that the convective heat transfer contribution plays a minor role in these conditions. Similar trends are found for refrigerant R32, in which a typical convective behavior is observed only for the highest mass flux of 300 kg/(m^2 s). An increasing heat flux leads instead to a significant enhancement of the average heat transfer coefficients (+55% for R32 and +130% for R290 when passing from 10 to 40 kW/m^2), and also to a reduced vapor quality corresponding to the onset of dry-out.
- The two-phase heat transfer coefficient prediction method of Del Col [15] returns the best agreement when compared to the experimental data, providing a *MAE* of 19.6% and 24.6% when used with R32 and R290 points, respectively.
- When the same operating conditions are applied, the adiabatic frictional pressure gradients of R32 are lower (approximately three times) than those of R290, due to the higher reduced pressure that increases the vapor-to-liquid density ratio, reducing the shear stress between the two phases. For the same reason, the pressure drops of both fluids are lower with increasing saturation temperature. As expected, a higher mass flux provides instead a higher frictional pressure gradient, due an increased flow velocity and inertia.
- The two-phase frictional pressure drop correlation of Zhang and Webb [17] better predicts the R32 data (*MAE* = 21.5%, whereas the prediction method of Friedel [18] returns the best agreement with R290 experimental points (*MAE* = 21.4%).

Acknowledgements
Luca Viscito received a grant at Federico II University funded by “Ministero dell’Istruzione dell’Università e della Ricerca”, via the project PRIN2015 “Clean Heating and Cooling Technologies For An Energy Efficient Smart Grid”, which is gratefully acknowledged.

References

[1] Regulation (EU) No 517/2014 of the European Parliament and the Council of 16 April 2014 *Off. J. Union*
[2] Botticella F, de Rossi F, Mauro A W, Vanoli G P and Viscito L 2018 *Int. J. Ref.* **87** 131-153
[3] Mastrullo R, Mauro A W, Menna L and Vanoli G P 2014 *En. Conv. Manag.* **82** 54-60
[4] Fernando P, Palm B, Lunqvist P and Granryd E 2004 *Int. J. Ref.* **27** 761-773
[5] Xu X, Hwang Y and Radermacher R 2013 *Int J. Ref.* **36** 892-903
[6] Longo G A, Mancin S, Righetti G and Zilio C 2017 *Appl. Th. Eng.* **124** 707-715
[7] Wang S, Gong M Q, Chen G F, Sun Z H and Wu J F 2014 *Int J. Ref.* **41** 200-209
[8] Del Col D, Bortolato M and Bortolin S 2014 *Int J. Ref.* **47** 66-84
[9] Longo G A, Mancin S, Righetti G and Zilio C 2016 *Int J. Ref.* **61** 12-22
[10] Jige D, Sagawa K and Inoue N 2017 *Int. J. Ref.* **76** 206-218
[11] Lillo G, Mastrullo R, Mauro AW and Viscito L 2018 *Int J Heat Mass Tr.* **126** 1236-1252
[12] Moffat R J 1982 *Trans. ASME: J. Fl. Eng.* **104** 250-260
[13] Dittus F W and Boelter L M K 1930 *Univ. Calif. Publ. Engin.* **2** 443-461
[14] Wojtan L, Ursenbacher T and Thome J R 2005 *Int. J. Heat Mass Tr.* **48** 2970-2985
[15] Del Col D 2010 *Exp. Th. Fluid Sc.* **34** 234-245
[16] Gungor K and Winterton R 1986 *Int. J. Heat Mass Tr.* **29** 351-358
[17] Zhang M and Webb R L 2001 *Exp. Th. Fluid Sc.* **25** 131-139
[18] Friedel L 1979 *Proc. In: Europ. Two Phase Flow Group Meeting* **E2** 485